Theoretical Insights for Improving the Schottky-Barrier Height at the Ga_2O_3/Pt Interface

Félix Therrien,[1,2] Andriy Zakutayev,[2,1] and Vladan Stevanović[1,2,*]

[1] *Colorado School of Mines, Golden, Colorado 80401, USA*

[2] *National Renewable Energy Laboratory, Golden, Colorado 80401, USA*

(Received 17 August 2021; revised 30 October 2021; accepted 22 November 2021; published 28 December 2021)

In this work, we study the Schottky-barrier height (SBH) at the junction between β-Ga_2O_3 and platinum, a system of great importance for the next generation of high-power and high-temperature electronic devices. Specifically, we obtain interfacial atomic structures at different orientations using our structure-matching algorithm and compute their SBH using electronic structure calculations based on hybrid density-functional theory. The orientation and strain of platinum are found to have little impact on the barrier height. In contrast, we find that decomposed water molecules (H.OH), which could be present at the interface from Ga_2O_3 substrate preparation, has a strong influence on the SBH, in particular in the $(\bar{2}01)$ orientation. The SBH can range from approximately 2 eV for a pristine interface to nearly zero for a full H.OH coverage. This result suggests that a SBH of approximately 2 eV can be achieved for the $Ga_2O_3(\bar{2}01)$/Pt junction using the substrate-preparation methods that can reduce the amount of adsorbed water at the interface.

DOI: 10.1103/PhysRevApplied.16.064064

I. INTRODUCTION

It is estimated that, currently, about 30% of all electricity in the United States goes through high-power electronic devices such as the ac-dc and dc-ac converters used in battery chargers, power supplies, etc. [1] This proportion could rise up to 80% in the next decade [2], given the expected proliferation of renewable-energy technologies, modernization of the power grids, and the transition to electric transportation. Therefore, even marginal gains in power-device efficiency could have a major impact on the aggregate energy consumption.

Wide-band-gap semiconductors such as SiC, GaN and Ga_2O_3, with their higher breakdown fields and good conductivity, have emerged as alternatives to standard inexpensive, but difficult to engineer, Si-based power devices [3]. In particular, β-Ga_2O_3 has been identified as the fourth generation of high-power electronic materials because of its relatively low projected cost [4], wide band gap (4.8 eV) [5,6], large breakdown field, and high permittivity, which together give it one of the highest Baliga figures of merit [7,8], the performance indicator for high-power electronics. In addition to high-temperature and high-power electronics, Ga_2O_3 has applications in gas (humidity) sensing [9,10], solar-blind photodetection [11], (photo)catalysis [12,13], electroluminescence [14,15], and many others [16,17]. Because of its unique properties, it has received significant attention from the research community in recent years [16].

Limited doping, however, puts some limitations on the architecture of Ga_2O_3-based devices. Namely, it is currently possible to dope Ga_2O_3 *n* type, while *p*-type-doped Ga_2O_3 is nearly impossible to attain [18,19]. In fact, wide-band-gap and bipolar materials are generally very hard to come by [20]. Consequently, device prototyping has focused mainly on (unipolar) Schottky-barrier diodes (SBD) and metal-oxide–semiconductor field-effect transistors (MOSFETs) [21]. Both rely on the formation of an electric charge depletion region, a Schottky barrier, at the interface between a metal and the semiconductor (here, *n*-type-doped β-Ga_2O_3). Its height determines the electrical (rectifying) characteristics of the contact. A large Schottky-barrier height (SBH) is ideal for diodes that require low current under reverse bias (leakage current). On the other hand, a near-zero SBH, where current flows freely through the interface in both directions, is ideal for passive (or Ohmic) electrical contacts.

Considering the importance of the SBH for high-power devices, revealing the factors that govern it as well as offering strategies on how to improve it (increase or lower depending on the need) would be invaluable. Specifically, for the β-Ga_2O_3/Pt junction studied here, the identification of a procedure to obtain a large SBH leading to a low leakage current would potentially have a lasting impact on future Ga_2O_3-based power devices [22,23]. In this work, we investigate the Schottky barrier at the β-Ga_2O_3/Pt

*vstevano@mines.edu

 © 2021 American Physical Society

junction using atomistic computational methods. We use our structure-matching algorithm [24] to provide the best-matching interface structures between platinum and two orientations of gallium oxide, $(\bar{2}01)$ and (100). These structures are then used as inputs for electronic calculations at the hybrid density-functional theory (DFT) level, which provide a means to evaluate the barrier heights. We find SBHs of approximately 2 eV for β-$Ga_2O_3(\bar{2}01)$/Pt and approximately 1.5 eV for β-$Ga_2O_3(100)$/Pt, in comparison with the experimentally measured values of approximately 1 eV and approximately 1.4 eV, respectively. We then show how the presence of adsorbed dissociated water at the interface can significantly reduce the measured SBH for the β-$Ga_2O_3(\bar{2}01)$/Pt interface but has little impact on β-$Ga_2O_3(100)$/Pt, which could explain the discrepancy between predicted and measured values in the $(\bar{2}01)$ orientation.

Finally, we investigate how the Pt orientation and strain influence the results and find that neither has an appreciable impact on the predicted barrier heights. The results presented in this paper highlight the important role of surface adsorbates on electrical contact properties and provide an insight into improving the performance of future Ga_2O_3 devices.

II. METHODS

The workflow used in this paper is depicted in Fig. 1. We start from the crystal structure of β-Ga_2O_3 (a conventional unit cell with 20 atoms, shown in Fig. 1) and the face-centered-cubic (fcc) platinum. Here, we choose platinum because of its high work function, which in general leads to higher Schottky barriers. On the β-Ga_2O_3 side (left), we first cut the structure along the specific orientation that we wish to study. We are particularly interested in the $(\bar{2}01)$ orientation of β-Ga_2O_3 because of previous experimental work [25,26]. We also investigate the (100) orientation, which is the most stable, primarily to validate our approach against previous studies [27]. Both of these orientations have multiple possible surface terminations. We choose the

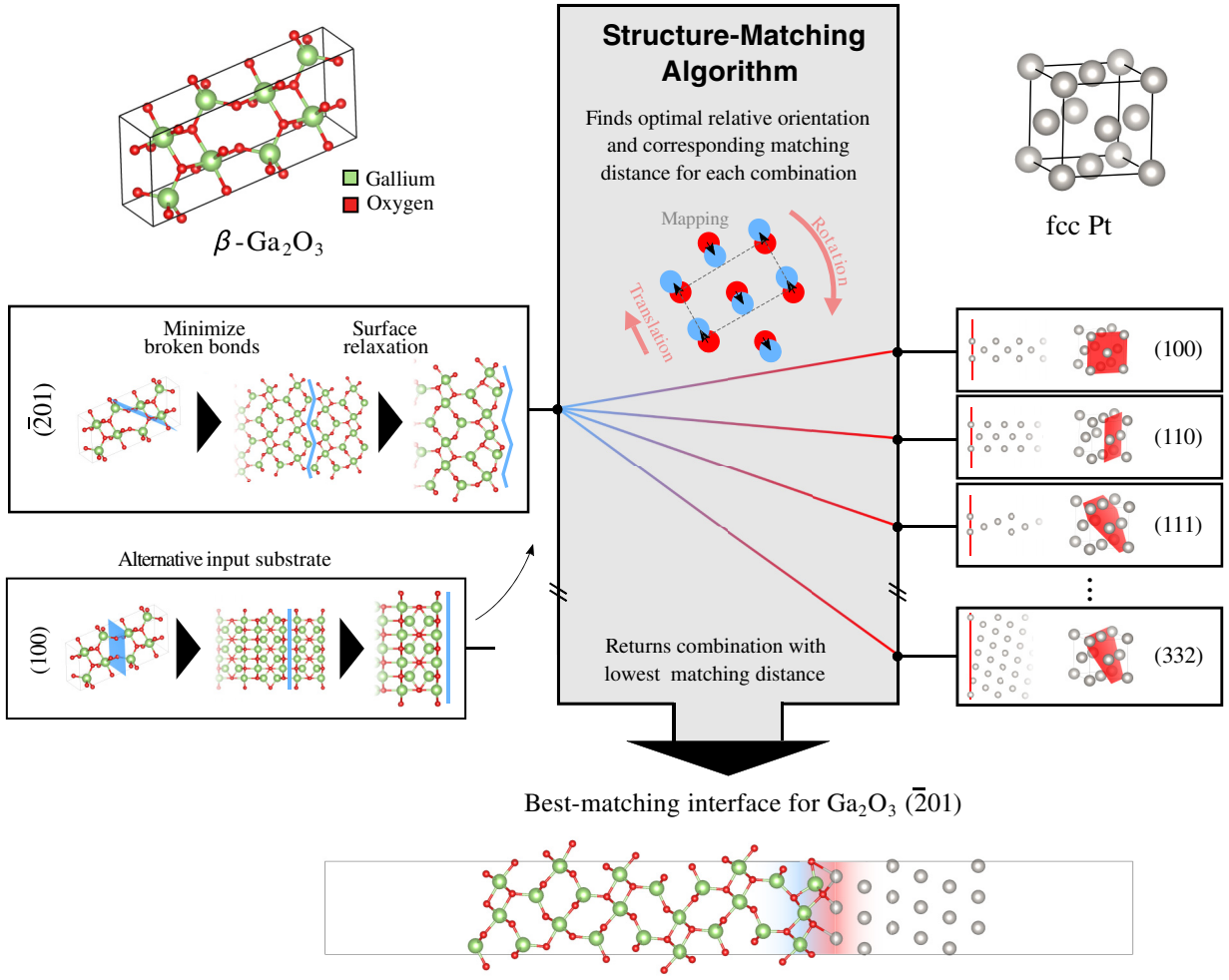

FIG. 1. The workflow to construct interfacial atomic structures. The structure-matching algorithm represented by the box in gray takes as an input a β-Ga_2O_3 surface (left) and a set of Pt surfaces (right). It returns the interface structure of the best matching combination of interfaces.

terminations that minimize the number of broken bonds, where the bonds are defined geometrically as those within the first coordination shell. This choice of termination has previously been shown to result in ionization potentials and electron affinities that compare well with the measured ones for a range of semiconductor materials [28,29]. As shown on the left of Fig. 1, the terminations do not necessarily have to be planar and can be corrugated (jagged blue line). In order to simulate surfaces (and interfaces), we create slabs of several layers of gallium oxide that are periodic parallel to the specified plane, $(\bar{2}01)$ or (100), but finite in the direction normal to that plane. Each slab is separated by 20 Å of vacuum such that there is no interaction between them. Since the slabs should ideally be semi-infinite, they are made to be as thick as computationally affordable. Once the surfaces are chosen, they are relaxed using DFT The relaxed β-Ga_2O_3 structure is then fed into the structure-matching algorithm described hereafter.

On the platinum side (right of Fig. 1), there is always only one possible termination because there is a single atom in the fcc unit cell. We do not relax the surfaces because, in experiment, the metal is deposited directly onto the gallium oxide without ever forming a surface. We feed the algorithm every possible symmetry-inequivalent orientation of platinum within the Miller index limits $-3 \leq h, k, l \leq 3$. For each of these orientations, we compute the "goodness of match" (described below), which then provides the best-matched interface structures.

Finally, once the best Pt/Ga_2O_3 matching structures are found for $(\bar{2}01)$ and (100), we passivate the outside surface of the gallium oxide using partial H atoms such that there are no surface states or dipoles at the outside surface. We relax the full structure except for the layer of oxygen that is furthest from the interface using DFT. In all the DFT calculations, we use the generalized-gradient approximation (GGA) with the Perdew-Burke-Ernzerhof (PBE) functional and the projector-augmented-wave (PAW) pseudopotentials as implemented in the VASP software package [30–32]. We calculate the electronic properties with the Heyd-Scuseria-Ernzerhof (HSE06) functional [33] to obtain a more realistic description of the electronic structure including the band gaps and to compute the SBH.

A. Matching crystal structures

The structure-matching algorithm, detailed in Ref. [24], minimizes a given cost function (e.g., total displacement of all atoms, energy, etc.) with respect to the atom-to-atom mapping and relative orientation of two sets of atoms. It has been shown to successfully find optimal transformation pathways between two materials [34]. In Ref. [24], we have demonstrated that structure matching can also be used to find the orientation relationship and bonding pattern at two semicoherent heterointerfaces: SiC(110)/Si(001) and YSZ(111)/Ni(111), where "YSZ" denotes yttria-stabilized zirconia. In the current work, we use an improved version of this algorithm to find the best matching and orientation relationships between the termination planes of platinum and β-Ga_2O_3.

To find the optimal structure, the algorithm goes through each combination of termination planes as illustrated in the center of Fig. 1: β-$Ga_2O_3(\bar{2}01)$/Pt(100), β-$Ga_2O_3(\bar{2}01)$/Pt(110), β-$Ga_2O_3(\bar{2}01)$/Pt(111), etc. For each combination, the matching is performed in the following way. First, two large spherical [in two-dimensional (2D) circular] sections of the two crystals with approximately 300–450 atoms are created. One set contains only the oxygen atoms that are at the surface of the gallium oxide and the other contains only the surface platinum atoms. In both cases, only atoms that are within 1 Å of the surface are considered. These sets are then matched directly without using any information related to the periodicity of the two crystals. Each oxygen atom is mapped to a platinum atom in an optimal manner using the Kuhn-Munkres algorithm [35]. The quantity that is being optimized is a two-body Lennard-Jones potential with an equilibrium radius of 2.5 Å. In an iterative process, the total Lennard-Jones energy (the "goodness-of-matching" function) is simultaneously minimized with respect to the relative orientation (angle), in-plane strain, and atom-to-atom mapping (choice of a "bonding" pattern) between the two surfaces.

The strains and the rotation angle are represented by a 2×2 transformation matrix. In this case, we limit the amount of strain to 8% in each in-plane direction (principal strain): it can be either tensile or compressive. We apply the strain fully on the platinum side of the interface, leaving the β-Ga_2O_3 intact. In the final step, once the optimal match is found, the periodicity of the mapping is retrieved, i.e., the 2D unit cell (represented by a 2×2 matrix $C_{Ga_2O_3}$) that is common to both structures in their optimal orientation is found. This step can have the effect of increasing the strain above the threshold (8%) such that the transformation matrix is exactly commensurate with both unit cells: $C_{Ga_2O_3} = TC_{Pt}$, where $C_{Ga_2O_3}$ and C_{Pt} are supercells of the β-Ga_2O_3 and Pt in-plane unit cell, respectively. For each combination, an optimal total bonding energy is obtained: its absolute value has no physical meaning but it can be used to compare the quality of the match. As noted already, this procedure has been shown to produce realistic interface structures. The effect of strain is discussed later in the text. The structure-matching algorithm used here is available in the form of an open-source software package called P2PTRANS [36].

B. Computing the Schottky-barrier height

Over the past century, many models have been developed to describe the physics of the Schottky barrier. Schottky [37] and Mott [38] estimated that the

SBH was equal to the difference between the work function of the metal and the electron affinity of the semiconductor (known as the Schottky-Mott rule). In other words, the bands are aligned such that the vacuum levels of the metal and the semiconductor coincide. Even though the simplicity of this model makes it a popular pedagogical tool to understand the formation of the barrier, it is unable to accurately describe most physical interfaces. Bardeen developed a more complex interface model that took into account the presence of surface states in the band gap of the semiconductor [39], which has led to the well-known Cowley-Sze equation [40]. This theory explains how the existence of surface states may cause "Fermi-level pinning" but it relies on the existence of a physical gap between the semiconductors and the metal. In reality, the surfaces are close enough that surface states cannot remain unchanged (they become interface states) and the physical boundaries of the two materials are difficult to define. To account for this problem, the metal-induced gap states (MIGS) theory [41–43] has been proposed. It adapts Bardeen's theory to systems with intimate interfaces by replacing the gap between the materials with the length of the MIGS tails. However, there are doubts on the physical relevance of this adaptation [44]. Detailed accounts of Schottky-barrier theories can be found in Refs. [44,45].

More recently, SBH is computed using first-principles electronic structure methods, typically DFT, by effectively measuring the difference in energy between the conduction-band minimum (CBM) in the semiconductor and the Fermi energy of the metal-semiconductor (MS) system at the actual (model) interface [27,46–50]. Unlike the Schottky-Mott rule, this method does take into account changes in the electronic structures of two materials due to interface formation. This is the method that we use in this paper. The approach implicitly makes the assumption that the band alignment at the interface—determined with DFT, or in our case, the hybrid HSE06 functional—remains completely unchanged by the doping of the semiconductor.

The use of the plane-wave basis in the electronic structure calculations poses two limitations. First, it requires a 2D periodic interface structure with a relatively small number of atoms (a couple of hundred). When there is no obvious lattice match and there is no known preferential orientation for the metal, it is difficult to choose an interface structure that is representative of the physical system. Because of that, it has remained challenging to assess the accuracy of *ab initio* calculation at predicting the SBH. By using structure matching to create interface structures, we can not only justify our choice of a representative interface structure but we can also relatively easily create interface structures in any orientation of Pt with varying numbers of atoms and measure their effect on the SBH. Such an analysis is presented later in this text. Second, the notorious band-gap underestimation of the standard approximations to DFT, namely the local-density approximation (LDA) and the GGA, also make computations of the SBH difficult. However, it is presently possible to use more accurate and more computationally demanding electronic structure methods, such as the hybrid functions, on systems with many hundreds of atoms and to overcome the limitations enforcing the use of the LDA and the GGA. In this way, a truly predictive method to compute the SBH can be constructed, which is precisely what we are showcasing in this paper.

III. RESULTS

The average Lennard-Jones (LJ) energy or goodness of match computed per the Pt-O pair of mapped atoms (i.e., the Lennard-Jones "bond") between β-Ga_2O_3 $(\bar{2}01)$ and the 13 orientations of platinum with Miller indices between -3 and 3 is shown in Fig. 2(a). This is the output from the structure-matching algorithm: the lower value, the better the match. The full length of each bar represents the average goodness of match per LJ bond when the Pt surface is strained. However, this does not account for the cost in energy from straining the Pt lattice to obtain the best-matched interface. To quantify that effect, keeping the same bonds (mapping) at the interface, the strain in Pt is removed and the LJ energy is recomputed, i.e., instead of straining the Pt, the bonds at the interface are stretched to compensate for the difference in unit cells between the gallium oxide and the platinum. Doing so provides an upper limit for the LJ energy where there is no contribution from strain (the pale blue part of each bar). In other words, the

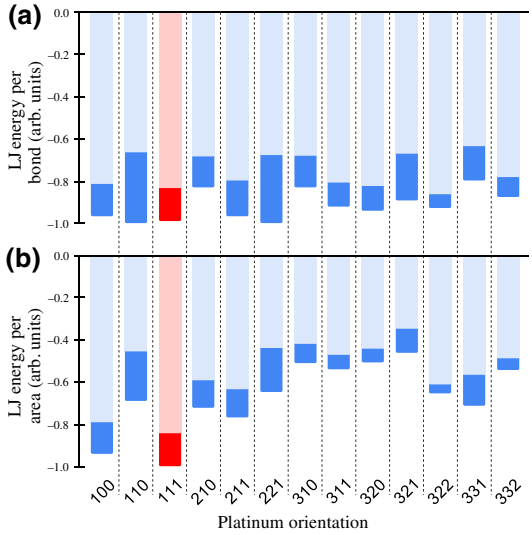

FIG. 2. The optimal Lennard-Jones energy ("goodness" of match) calculated between β-$Ga_2O_3(\bar{2}01)$ and all symmetry-inequivalent Pt planes with Miller indices between -3 and 3 (a) per pair of matched Pt-O atoms (i.e., the Lennard-Jones "bond") and (b) per unit area of the interface. The values are normalized to 1.

pale-blue portion of each bar corresponds to a situation where the materials would be so stiff that no amount of strain would be present at the interface and the mismatch between the two structures would be fully accommodated by the bonds at the interface. The full length of the bars (dark blue + pale blue), on the other hand, corresponds the situation where straining the atoms near the interface has no energetic cost up to the maximum allowed strain. The reality lies somewhere between the two (dark-blue region). The wider the dark-blue region, the more strained the optimal result is for each orientation.

Looking at Fig. 2(a), the Pt orientations that best match β-Ga_2O_3 $(\bar{2}01)$ in terms of the Pt-O mapping are (110), (221), (111), and (100), with (110) and (221) needing large strains to accommodate a near-perfect matching. Since the density of surface atoms is different for different orientations, it is more relevant to look at the LJ energy per unit of area [Fig. 2(b)], since it represents a proxy for the interface energy. When doing so, it becomes clear that the (111) orientation of Pt is the best-matching orientation, followed by (100). The optimal interface structure used in the rest of this paper, β-Ga_2O_3 $(\bar{2}01)$/Pt(111), is depicted in Fig. 3. As explained further in this section, the relatively high tolerance on strain allows for a smaller interface unit cell (shown in blue) where the hexagonal shape of the Pt(111) plane is distorted to match perfectly that of the β-Ga_2O_3 $(\bar{2}01)$ surface. Note that the interface in Fig. 3 is an atomistic model representation of the situation at flat β-Ga_2O_3 $(\bar{2}01)$ terraces. A more realistic representation of the microstructure, including steps, kinks, etc., would require a large interface structure that would hardly be tractable with *ab initio* methods.

After relaxation of the interface structure, all the Pt atoms move slightly away from the gallium oxide as the Ga atom that is closest to the interface moves toward the platinum, retrieving its original bulk position [see the bottom of Fig. 4(a)]. From this relaxed structure, we obtain the position-dependent local density of states (LDOS) by computing the charge density for 100 energy intervals between $E_f - 5$ eV and $E_f + 5$ eV, where E_f is the Fermi energy. For each interval, we integrate the charge density in plane to obtain the density of states as a function z along the interface structure. The LDOS for the relaxed interface structure between β-$Ga_2O_3(\bar{2}01)$ and Pt(111) along with the relaxed crystal structure are presented in Fig. 4(a). The band gap in gallium oxide is approximately 4 eV, which is an underestimate compared to the experimental value (4.8 eV). This difference is due to the remaining underestimation of HSE for DFT-relaxed β-Ga_2O_3. For a more detailed discussion on the band gap in slabs of finite sizes, see the Supplemental Material [51].

In Fig. 4(a), we can directly measure the SBH from the Fermi energy to the CBM on the gallium oxide side, by assuming that the CBM is the first visible state (pale blue) that spans the entire gallium oxide structure. We predict

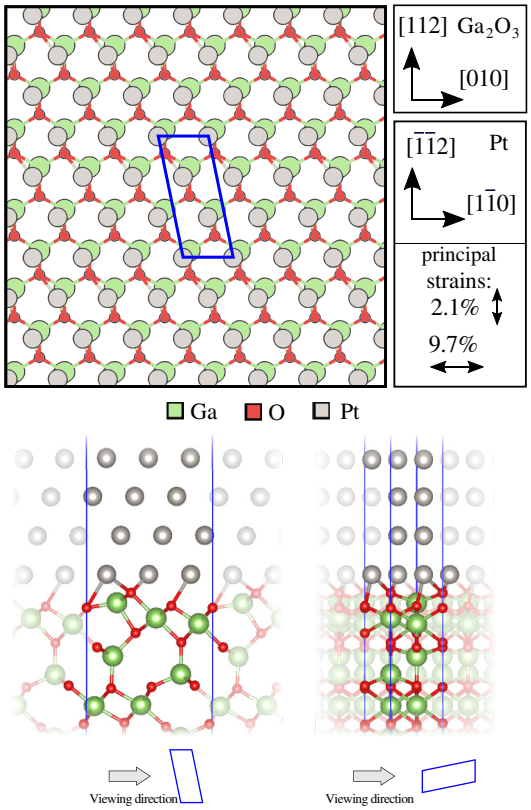

FIG. 3. The optimally matched interface structure between β-Ga_2O_3 $(\bar{2}01)$ and Pt(111) corresponding to the red bars in Fig. 2. The in-plane periodic unit cell of the interface is represented by a blue parallelogram. Outward-pointing arrows indicate tensile strain. The strains apply to Pt only.

a SBH of approximately 1.9 eV. Since the band gap is somewhat underestimated, we can expect that the true SBH would be slightly higher, an effect that would be compensated in part by the image-charge effect, which is of the order of 0.1–0.2 eV [52,53], depending on the level of doping and the applied voltage. Even with the underestimated band gap, this is much larger than the reported experimental SBH for that interface, of 1.05 eV [from current-voltage (I-V) characteristics] [54,55]. We also obtain the position of the CBM and the valence-band maximum (VBM) by shifting the bulk values by an amount corresponding to the average electrostatic potential in gallium oxide and obtain the same SBH (see the Supplemental Material [51]). Here, as others have done before [27,46–50], we make the assumption that the position of the CBM with respect to the metal energy levels at the interface does not change with doping. We do not expect to see any appreciable band bending at this scale, since the depletion region is much larger than the structures used here. If we were able to see it, the bands of doped gallium oxide would bend down such that the Fermi level would be close to the CBM far away from the interface.

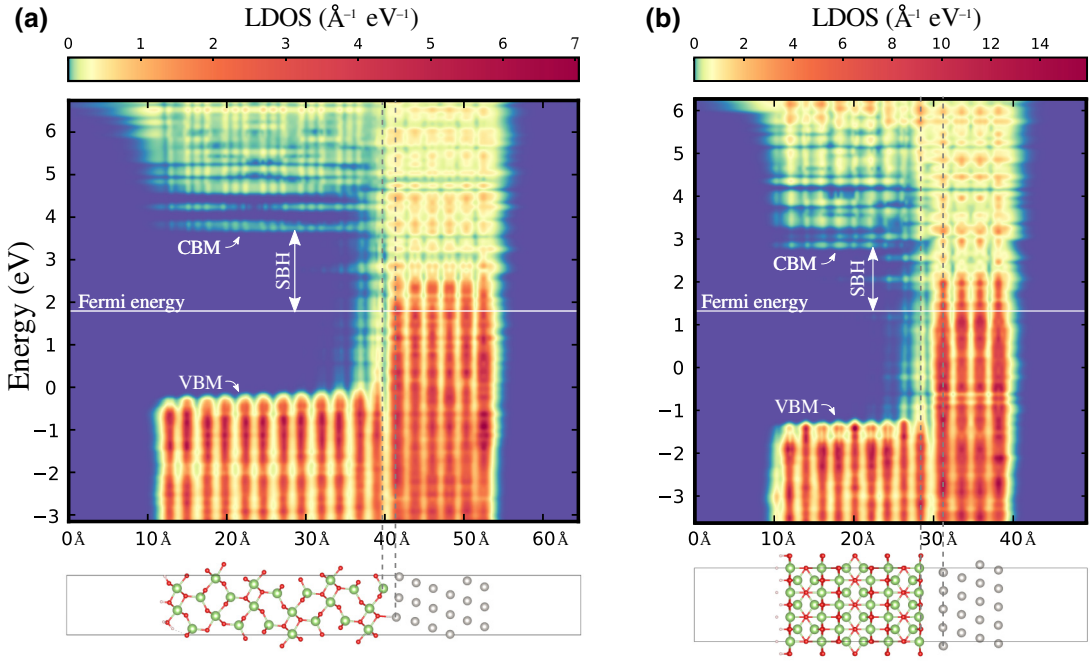

FIG. 4. The LDOS for (a) the β-Ga_2O_3 $(\bar{2}01)$ and Pt(111) interface and (b) the β-Ga_2O_3(100) and Pt(111) interface. The Fermi energy is shown as a white line and the x axis is in line with the corresponding relaxed structure.

In order to validate our method, we apply the same workflow (Fig. 1) to the (100) orientation of β-Ga_2O_3, which has been studied both experimentally [56] and computationally [27]. From structure matching, we once again obtain Pt(111) as the optimal match. This is the same Pt orientation that is used in Ref. [27], where it is chosen based on the fact that it is commonly used in experiment. Ga_2O_3 (100) being a very stable surface, relaxation of the surface and the interface structure do not significantly change the atomic layout. The LDOS of the relaxed interface structure is presented in Fig. 4(b). One may note that the band gap in the (100) orientation is slightly larger than in the $(\bar{2}01)$ orientation. This can be explained by spurious finite-size effects that are more important in the (100) orientation, which is thinner despite requiring more atoms (for more details, see the Supplemental Material [51]). In this case, the SBH is significantly lower, at 1.5 eV. This value is much closer to experimental measurements in that orientation, 1.4 eV (from I-V characteristics) [56], and the theoretical estimate of 1.4 eV obtained by Xu *et al.* with nearly identical parameters. This provides confidence in our ability to predict the SBH but it begs the question "Why is the predicted SBH in the $(\bar{2}01)$ so much higher than the one measured in experiment?"

A. Adsorption of water products

To answer this question, we look at possible contaminants that could have been adsorbed at the surface during preparation and could have an influence on the SBH. Since the β-Ga_2O_3 samples are usually washed with deionized water before platinum is deposited [25,26], we focus on waterlike products. Moreover, commercially available β-Ga_2O_3 $(\bar{2}01)$ substrates are known to be H and OH terminated [57]. Therefore, to model this situation, we create a structure where the two broken bonds per unit cell at the Ga_2O_3 surface are connected to H^+ and OH^- groups, forming a decomposed water molecule (H.OH). The actual surface may contain varying proportions of H and OH depending on the treatment, most of them coming in equal parts from the decomposition of water molecules [57–59]. Since we focus on the typical deionized-water treatment, the proportion of 50% is appropriate. It also has the important advantage of being charge neutral.

Upon relaxation, the decomposed water remains stable at the surface. We then add the Pt layers in the same orientation as in Fig. 4(a). Once again, the decomposed water remains stable upon relaxing the interface. Note that, after relaxation, the attached OH^- at the interface is almost parallel to the surface [see the inset of Fig. 5(b)], which is consistent with previous work [58].

The LDOS of that interface is shown in Fig. 5(a). It is immediately evident that the SBH is reduced to practically zero by the presence of the adsorbed decomposed water; the Fermi energy sits directly under the CBM. In Fig. 5(b), the electrostatic potential of the β-$Ga_2O_3(\bar{2}01)$/H.OH/Pt(111) interface, in blue, and the electrostatic potential of the β-Ga_2O_3 $(\bar{2}01)$/Pt(111) interface, in gray, are overlaid using the vacuum level on the Pt side as a reference. One can see that the entire electrostatic

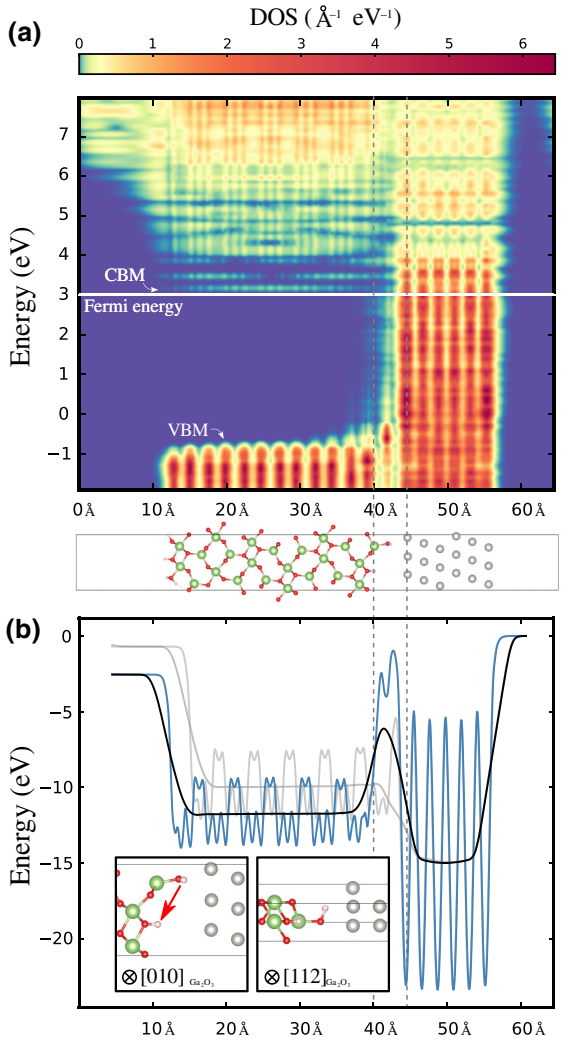

FIG. 5. The electronic properties of a β-$Ga_2O_3(\bar{2}01)$ /H.OH/Pt(111) interface. (a) The LDOS, showing the Fermi energy as a white line. (b) The electrostatic potential in blue, with its average in black. The pale-gray lines are the electrostatic potential and the average electrostatic potential for the interface shown Fig. 4(a). The inset in (b) shows an enlarged view of the interface from two directions. The red arrow shows the direction of the dipole between OH and H (in the physics convention).

potential on the gallium side of the interface is shifted by an amount corresponding to the SBH in Fig. 4(a). The average potential on both sides of the interface remains flat, which means that the additional dipole that causes the shift in potential is located at the interface. This added dipole illustrated in the inset of Fig. 5 goes from the negatively charged OH^- to the positively charged H^+ on the corrugated Ga_2O_3 surface.

In Fig. 5, the concentration of adsorbed H.OH is very high; it assumes that every single interface cell (Fig. 3) adsorbs one water molecule. Therefore, certain properties of the interface structure in Fig. 5 are not representative of the real interface, where the concentration of adsorbed water is much lower. For example, there is a large physical gap between the Pt atoms and the Ga_2O_3 atoms in Fig. 5; in reality, this gap would be present only close to the OH group and Pt atoms far away from it would be closer to Ga_2O_3, as in Fig. 4(a). In the same way, the measured SBH of the full interface would likely fall between that of Fig. 4(a) and that of Fig. 5. One way to estimate the effective Schottky barrier is to compute the shift in electrostatic potential due to a finite concentration of dipoles at the interface. For example, using the position of the added H and O atoms and by solving the Poisson equation in one dimension, we can estimate the charge density necessary to shift the dipole by 0.85 eV (to go from the ideal 1.9-eV to the experimental 1.05-eV barrier). We find that there would need to be about one adsorbed H.OH every 14 unit cells (5.3×10^{-11} mol/cm^2) to obtain a SBH of 1.05 eV. This offers a simple understanding of the concept of effective SBH in the presence of surface dipoles.

Another interpretation is that the barrier itself is inhomogeneous, consisting of regions with high SBH corresponding to the interface in Fig. 4(a) and smaller regions with low SBH corresponding to the interface in Fig. 5 (or other interface defects). The effective or apparent SBH of the device, measured in experiment, would lie between the two values depending on the concentration of adsorbed water and the experimental method used to measure the SBH [60,61]. In fact, regions of the surface ("patches") with low SBH have a strong effect on the observed *I-V* behavior of the device and consequently the measured value of the barrier height [61].

There are two ways to experimentally measure the SBH: using the capacitance-voltage (*C-V*) characteristics or using the *I-V* characteristics. Measurements using the *C-V* characteristics are less sensitive to fluctuations and closer to the average SBH, whereas *I-V*–based measurements are more representative of the effective barrier for current flow [54,62]. For example, Ref. [54] has reported a barrier height of 1.05 eV using the *I-V* characteristics and a barrier height of 1.9 eV using the *C-V* characteristics. This is consistent with our result: since the concentration of adsorbed H.OH is low, the average SBH measured with the *C-V* characteristics is near the calculated ideal value of 1.9 eV, whereas the effective value measured with the *I-V* is strongly reduced by the presence of a few near zero patches. Note that the exactitude of the agreement of the *C-V* measurement with our predicted value (1.9 eV in both cases) may depend on small differences in experimental preparation, since a more recent study [55], which has also measured 1.05 eV with the *I-V* characteristics, has found a 1.20-eV SBH with the *C-V* characteristics.

As mentioned before, the (100) surface is more stable than the $(\bar{2}01)$ surface. We compute their energies to be about 0.03 eV/Å^2 and 0.06 eV/Å^2, respectively, in agreement with other theoretical data [58]. This difference in surface energy has an influence on their respective growth

rate [63] and their ability to adsorb water products during surface preparation. In fact, the adsorption of H.OH on the (100) surface is unstable with respect to the adsorption of water [59,64], which could explain why our estimate of the SBH in the (100) orientation is more accurate: there are simply not as many H.OH on the surface to reduce the effective barrier height. To quantity the effect of adsorbates in the (100) orientation, we create a β-Ga_2O_3 (100) surface with H.OH by connecting the six broken bonds per unit cell with H^+ and OH^- (three with H^+ and three with OH^-), as we do for the (111) surface (which has two broken bonds). The structure is stable after initial relaxation but one of the three H.OH recombines to form a water molecule upon adding the Pt layers. We compute the LDOS of that interface and find that the addition of H.OH (two H.OH and one H_2O molecule after relaxation) has no significant impact on the barrier height, which further demonstrates that the presence of waterlike products on that surface has a less significant impact on the SBH.

The fact that H^+ and OH^- at the $(\bar{2}01)$ β-Ga_2O_3 surface have a strong influence on the SBH could explain why surface treatment with acids has been shown to increase the measured barrier height [54]. This means that the apparent barrier height of an acid-cleaned interface with less OH would be higher because of the reduction in the number of patches with near-zero effective barrier heights. Our results suggest that surface preparation should aim at reducing the presence of decomposed water on the surface as much as possible, which offers a route to obtaining a high Schottky barrier without adding any additional dipole layers (e.g., $PdCoO_2$ [22]). Methods that avoid the use of water completely should be considered.

Other preparation methods such as annealing in oxidizing conditions and oxygen-plasma treatment are known to have an important impact on the rectifying properties of metal-oxide interfaces. These methods contribute to removing oxygen vacancies near the oxide surface, which has been shown to influence the Schottky and/or Ohmic behavior of other metal-oxide devices [65–68]. Yet, they may also reduce water-product adsorbates at the surface. For example, it has been found that most of the measured increase in SBH that results from oxygen-plasma treatment of ZnO in a ZnO/Au interface is attributable to the removal of surface adsorbates, the reduction of oxygen vacancies having only a small impact [65]. This means that some effects associated with the reduction of oxygen vacancies may in fact be due to the phenomena discussed in this paper. In the same way, it is possible that oxygen vacancies in Ga_2O_3 play a role in explaining the observed discrepancy between the predicated and measured SBH discussed here. In fact, studies have found that oxygen vacancies can change the Schottky behavior of other Ga_2O_3-metal systems [69–71].

However, we believe that the presence of water adsorbates discussed in this section is the dominant effect, since the removal of oxygen vacancies has a relatively small impact on the SBH itself [71]. The change in rectifying properties is mainly due to the change in tunneling width [65,69,71] (or Schottky-barrier width), which is an important interface property that is independent of the SBH. Additionally, the presence of oxygen vacancies cannot easily explain the differences between the predicted (100) and $(\bar{2}01)$ barrier heights. Moreover, it has been shown experimentally that the presence of H and OH at the $(\bar{2}01)$ Ga_2O_3 surface changes the band bending near the surface by as much as 1 eV [57,72], which is of the same magnitude as the effect measured here. The study of the underlying mechanisms through which oxygen vacancies change the rectifying properties of our system would be an interesting research avenue. In any case, an approach such as oxygen-plasma treatment should be considered to improve the general rectifying properties of the interface, as it has a positive effect on both phenomena, i.e., it removes adsorbates while creating oxidizing conditions to fill oxygen vacancies.

B. Effect of strain and platinum orientation

To show the effect of the choice of the maximal allowable strain when matching interfaces and to provide confidence in our result, we compare best-matching interfaces with different strain tolerances. Let us focus on two structures between β-Ga_2O_3 $(\bar{2}01)$ and Pt(111): one with a strain of less than 8%, used throughout this paper and presented in Fig. 3, and one with a strain of less than 2.5%, presented in Fig. 6(a). In both cases, the in-plane strain is fully applied to the platinum side of the interface; gallium oxide retains its DFT-relaxed in-plane lattice parameters.

We calculate the SBH for the interface with less than 2.5% strain and find a value of 2.4 eV. Although it is a slightly higher value than the 1.9 eV for 8% strain, it is consistent with the overestimation of the SBH and it can be explained in part by the more important finite-size effects caused by the thinner Ga_2O_3 that is required to complete the calculation with this larger cell.

Note that one of the principal strains in Fig. 3 is higher than 8% and that one of the principal strains in Fig. 6 is higher than 2.5%. This is because the final interface unit cell must be a supercell of both the unit cells of gallium oxide and platinum, as illustrated in Figs. 6(b) and 6(c). This condition is true only for specific principal strains where vertices of the strained Pt and Ga_2O_3 coincide; in Fig. 3, the principal strains of 9.7% and 2.1% are the closest ones to the optimized strains—which are necessarily lower than 8%—that fulfill this condition.

The advantage of allowing for a higher strain is that the resulting interface structures are smaller, which is desirable for *ab initio* calculations. In Figs. 3 and 6(c), the interface cell, in blue, is comprised of only one β-Ga_2O_3 $(\bar{2}01)$ cell. In comparison, the optimal interface unit cell with

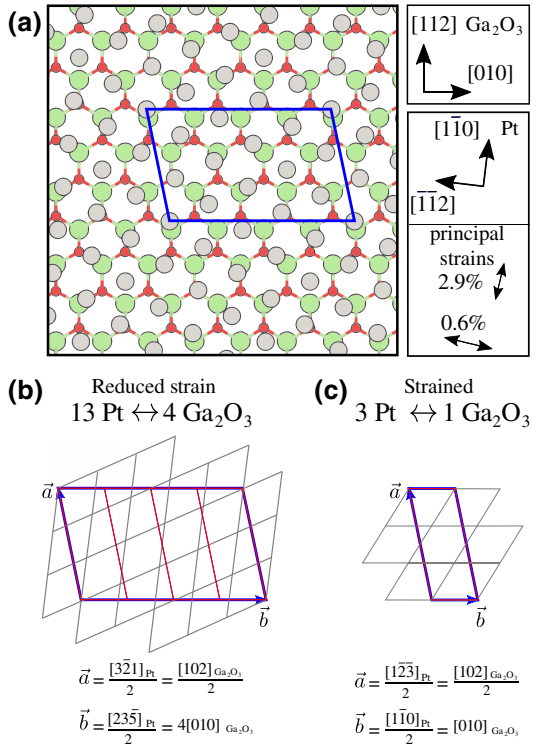

FIG. 6. The low- and high-strain β-Ga_2O_3 ($\bar{2}$01) and Pt(111) interfaces. (a) A a top view of the best-matching interface with a lower strain (stricter constraint). (b),(c) The orientation of the in-plane unit cell in terms of the Ga_2O_3 and Pt coordinates for (b) the reduced strain case and (c) the case with higher strain used throughout this paper. The in-plane unit cells of the interface structure, gallium oxide, and Pt are shown in blue, red, and gray, respectively. Outward-pointing arrows indicate tensile strain. The strains apply to Pt only.

strain, illustrated in Figs. 6(a) and 6(b), is composed of four β-Ga_2O_3 ($\bar{2}$01) unit cells. In that structure, the Pt is rotated by about 90° anticlockwise. The strain is 2.9% in one direction and close to zero in the other. As the strain tolerance decreases, the ratio of Pt to Ga_2O_3 changes. The high-strain structure [Fig. 6(c)] has a ratio of $1:3 = 33.33\%$, whereas the lower-strain structure [Fig. 6(b)] has a ratio of $4:13 = 30.77\%$. At even lower strains, this ratio would tend to 30.03%, the exact ratio of the specific areas between Pt(111) and β-Ga_2O_3($\bar{2}$01). In the same way as approximating an irrational number with an integer fraction requires larger integers for a higher precision, the size of the cell increases as the allowable strain decreases.

Finally, we evaluate the SBH for two other orientations in Pt: (221) and (321). We choose (221) because it has excellent bonding energy per bond [Fig. 2(a)] and a relatively good average energy per area [Fig. 2(b)]. It also has the particularity of having a sawtooth corrugated surface that is perfectly matched with the corrugated surface of gallium oxide. We choose the (321) surface because it is the worst-matching interface and hence we can see the effect of a "bad" match on the barrier height. For the (221) surface, we obtain a SBH of 1.9 eV and for the (321) interface, we obtain a SBH of 2.1 eV. These values do not differ significantly from the 1.9-eV barrier calculated for the Pt(111) orientation.

The test cases presented in this section give us better confidence that our main findings are applicable to real systems where Pt has no preferential orientation and where the strain at the interface might vary between different grains. The LDOS plots and their corresponding structures for all three interfaces presented in this section are available in the Supplemental Material [51].

IV. CONCLUSION

In this work, we create a plausible interface structure between fcc platinum and β-Ga_2O_3($\bar{2}$01) using structure matching [24]. We find that the best-matching orientation of Pt is (111). We then compute the LDOS of the newly created interface structure using DFT and predict a SBH of 1.9 eV, which is much higher than the experimentally measured value of 1.05 eV (I-V characteristics) [54,55]. To validate our methodology, we apply the same process to the (100) orientation of β-Ga_2O_3, which has been studied computationally [27] and experimentally [56], and find excellent agreement. Why is the predicted SBH so overestimated in ($\bar{2}$01) when it is relatively accurate in (100)? To answer this question, we create a β-Ga_2O_3 ($\bar{2}$01)/H.OH/Pt(111) interface and find that it has a zero barrier height (Ohmic behavior). The presence of decomposed water in some regions of the interface from conventional surface-cleaning methods could have the effect of reducing the effective SBH of the device, which would explain the discrepancy between the predicted and measured values of the SBH in the ($\bar{2}$01).

Our results are consistent with the fact that pretreatment of the β-Ga_2O_3 ($\bar{2}$01) surface with acids has a positive effect on the barrier height. They also confirm, as pointed out in Ref. [54], the importance of surface preparation during the fabrication of β-Ga_2O_3 devices. In fact, our results indicate that a perfectly clean β-Ga_2O_3($\bar{2}$01)/Pt interface could almost double the SBH (to approximately 2 eV). Since the barrier height of a metal-semiconductor interface is the property that has the most impact on its electrical characteristics [44], this could help the design and fabrication of high-power and high-temperature electronic devices with lower leakage current that could sustain larger breakdown fields.

Finally, we vary the strain and the orientation of the Pt and find that it has little impact on the predicted SBH. This shows how our approach using structure matching and the LDOS is useful in easily creating various interface structures and testing the influence of different physical parameters on the system. It offers a fully predictive and

convenient way to study electronic properties that can be applied to any solid-solid heterointerface.

ACKNOWLEDGMENTS

This work was authored in part at the National Renewable Energy Laboratory (NREL), operated by Alliance for Sustainable Energy, LLC, for the U.S. Department of Energy (DOE) under Contract No. DE-AC36-08GO28308. Funding was provided by the Office of Energy Efficiency and Renewable Energy (EERE) Advanced Manufacturing Office (AMO). Method development was supported by the National Science Foundation under Grant No. DMR-1945010. The research was performed using computational resources sponsored by the DOE's Office of Energy Efficiency and Renewable Energy located at NREL and using the Colorado School of Mines high-performance-computing resources. The views expressed in the paper do not necessarily represent the views of the DOE or the U.S. Government.

[1] L. Tolbert, T. King, B. Ozpineci, J. Campbell, G. Muralidharan, D. Rizy, A. Sabau, H. Zhang, W. Zhang, and Y. Xu *et al.*, Power electronics for distributed energy systems and transmission and distribution applications, ORNL/TM-2005/230, UT-Battelle, LLC, Oak Ridge National Laboratory (2005), Vol. 8, p. 1.

[2] C. F. Heuberger and N. Mac Dowell, Real-world challenges with a rapid transition to 100% renewable power systems, Joule **2**, 367 (2018).

[3] P. Gorai, R. W. McKinney, N. M. Haegel, A. Zakutayev, and V. Stevanovic, A computational survey of semiconductors for power electronics, Energy Environ. Sci. **12**, 3338 (2019).

[4] S. B. Reese, T. Remo, J. Green, and A. Zakutayev, How much will gallium oxide power electronics cost?, Joule **3**, 903 (2019).

[5] H. Peelaers and C. G. Van de Walle, Brillouin zone and band structure of β-Ga_2O_3, Phys. Status Solidi (b) **252**, 828 (2015).

[6] M. Orita, H. Ohta, M. Hirano, and H. Hosono, Deep-ultraviolet transparent conductive β-Ga_2O_3 thin films, Appl. Phys. Lett. **77**, 4166 (2000).

[7] M. Higashiwaki, K. Sasaki, A. Kuramata, T. Masui, and S. Yamakoshi, Gallium oxide (Ga_2O_3) metal-semiconductor field-effect transistors on single-crystal β-Ga_2O_3 (010) substrates, Appl. Phys. Lett. **100**, 013504 (2012).

[8] M. Higashiwaki, K. Sasaki, H. Murakami, Y. Kumagai, A. Koukitu, A. Kuramata, T. Masui, and S. Yamakoshi, Recent progress in Ga_2O_3 power devices, Semicond. Sci. Technol. **31**, 034001 (2016).

[9] L. Mazeina, F. K. Perkins, V. M. Bermudez, S. P. Arnold, and S. Prokes, Functionalized Ga_2O_3 nanowires as active material in room temperature capacitance-based gas sensors, Langmuir **26**, 13722 (2010).

[10] D. Wang, Y. Lou, R. Wang, P. Wang, X. Zheng, Y. Zhang, and N. Jiang, Humidity sensor based on Ga_2O_3 nanorods doped with Na^+ and K^+ from GaN powder, Ceram. Int. **41**, 14790 (2015).

[11] X. Chen, F. Ren, S. Gu, and J. Ye, Review of gallium-oxide-based solar-blind ultraviolet photodetectors, Photonics Res. **7**, 381 (2019).

[12] S. Jin, X. Wang, X. Wang, M. Ju, S. Shen, W. Liang, Y. Zhao, Z. Feng, H. Y. Playford, and R. I. Walton *et al.*, Effect of phase junction structure on the photocatalytic performance in overall water splitting: Ga_2O_3 photocatalyst as an example, J. Phys. Chem. C **119**, 18221 (2015).

[13] Y. Hou, L. Wu, X. Wang, Z. Ding, Z. Li, and X. Fu, Photocatalytic performance of α-, β-, and γ-Ga_2O_3 for the destruction of volatile aromatic pollutants in air, J. Catal. **250**, 12 (2007).

[14] T. Miyata, T. Nakatani, and T. Minami, Gallium oxide as host material for multicolor emitting phosphors, J. Lumin. **87**, 1183 (2000).

[15] P. Wellenius, A. Suresh, and J. Muth, Bright, low voltage europium doped gallium oxide thin film electroluminescent devices, Appl. Phys. Lett. **92**, 021111 (2008).

[16] S. Pearton, J. Yang, P. H. Cary IV, F. Ren, J. Kim, M. J. Tadjer, and M. A. Mastro, A review of Ga_2O_3 materials, processing, and devices, Appl. Phys. Rev. **5**, 011301 (2018).

[17] M. A. Mastro, A. Kuramata, J. Calkins, J. Kim, F. Ren, and S. Pearton, Perspective—opportunities and future directions for Ga_2O_3, ECS J. Solid State Sci. Technol. **6**, P356 (2017).

[18] H. Peelaers, J. L. Lyons, J. B. Varley, and C. G. Van de Walle, Deep acceptors and their diffusion in Ga_2O_3, APL Mater. **7**, 022519 (2019).

[19] A. Goyal, A. Zakutayev, V. Stevanović, and S. Lany, Computational fermi level engineering and doping-type conversion of Mg:Ga_2O_3 via three-step synthesis process, J. Appl. Phys. **129**, 245704 (2021).

[20] A. Goyal, P. Gorai, S. Anand, E. S. Toberer, G. J. Snyder, and V. Stevanović, On the dopability of semiconductors and governing material properties, Chem. Mater. **32**, 4467 (2020).

[21] H. Xue, Q. He, G. Jian, S. Long, T. Pang, and M. Liu, An overview of the ultrawide bandgap Ga_2O_3 semiconductor-based Schottky barrier diode for power electronics application, Nanoscale Res. Lett. **13**, 1 (2018).

[22] T. Harada and A. Tsukazaki, Control of Schottky barrier height in metal/*beta*-Ga_2O_3 junctions by insertion of $PdCoO_2$ layers, APL Mater. **8**, 041109 (2020).

[23] E. Farzana, Z. Zhang, P. K. Paul, A. R. Arehart, and S. A. Ringel, Influence of metal choice on (010) β-Ga_2O_3 Schottky diode properties, Appl. Phys. Lett. **110**, 202102 (2017).

[24] F. Therrien, P. Graf, and V. Stevanović, Matching crystal structures atom-to-atom, J. Chem. Phys. **152**, 074106 (2020).

[25] M. B. Tellekamp, K. N. Heinselman, S. Harvey, I. S. Khan, and A. Zakutayev, Growth and characterization of homoepitaxial β-Ga_2O_3 layers, J. Phys. D: Appl. Phys. **53**, 484002 (2020).

[26] K. Heinselman, P. Walker, A. Norman, P. Parilla, D. Ginley, and A. Zakutayev, Performance and reliability of β-Ga_2O_3

Schottky barrier diodes at high temperature, J. Vac. Sci. Technol. A: Vac. Surf. Films **39**, 040402 (2021).
[27] R. Xu, N. Lin, Z. Jia, Y. Liu, H. Wang, Y. Yu, and X. Zhao, First principles study of Schottky barriers at Ga_2O_3 (100)/metal interfaces, RSC Adv. **10**, 14746 (2020).
[28] V. Stevanović, K. Hartman, R. Jaramillo, S. Ramanathan, T. Buonassisi, and P. Graf, Variations of ionization potential and electron affinity as a function of surface orientation: The case of orthorhombic SnS, Appl. Phys. Lett. **104**, 211603 (2014).
[29] V. Stevanović, S. Lany, D. S. Ginley, W. Tumas, and A. Zunger, Assessing capability of semiconductors to split water using ionization potentials and electron affinities only, Phys. Chem. Chem. Phys. **16**, 3706 (2014).
[30] J. P. Perdew, K. Burke, and M. Ernzerhof, Generalized Gradient Approximation Made Simple, Phys. Rev. Lett. **77**, 3865 (1996).
[31] P. E. Blöchl, Projector augmented-wave method, Phys. Rev. B **50**, 17953 (1994).
[32] G. Kresse and J. Furthmüller, Efficiency of ab-initio total energy calculations for metals and semiconductors using a plane-wave basis set, Comput. Mater. Sci. **6**, 15 (1996).
[33] A. V. Krukau, O. A. Vydrov, A. F. Izmaylov, and G. E. Scuseria, Influence of the exchange screening parameter on the performance of screened hybrid functionals, J. Chem. Phys. **125**, 224106 (2006).
[34] F. Therrien and V. Stevanović, Minimization of Atomic Displacements as a Guiding Principle of the Martensitic Phase Transformation, Phys. Rev. Lett. **125**, 125502 (2020).
[35] H. W. Kuhn, The Hungarian method for the assignment problem, Naval Res. Logistics Q. **2**, 83 (1955).
[36] github.com/ftherrien/p2ptrans.
[37] W. Schottky, Zur Halbleitertheorie der Sperrschicht- und Spitzengleichrichter, Zeitschrift für Physik **113**, 367 (1939).
[38] N. F. Mott, The theory of crystal rectifiers, Proc. R. Soc. Lond. A Math. Phys. Sci. 171, 27 (1939).
[39] J. Bardeen, Surface states and rectification at a metal semiconductor contact, Phys. Rev. **71**, 717 (1947).
[40] A. Cowley and S. Sze, Surface states and barrier height of metal-semiconductor systems, J. Appl. Phys. **36**, 3212 (1965).
[41] V. Heine, Theory of surface states, Phys. Rev. **138**, A1689 (1965).
[42] C. Tejedor and F. Flores, A simple approach to heterojunctions, J. Phys. C: Solid State Phys. **11**, L19 (1978).
[43] J. Tersoff, Schottky Barrier Heights and the Continuum of Gap States, Phys. Rev. Lett. **52**, 465 (1984).
[44] R. T. Tung, The physics and chemistry of the Schottky barrier height, Appl. Phys. Rev. **1**, 011304 (2014).
[45] R. T. Tung, Recent advances in Schottky barrier concepts, Mater. Sci. Eng.: R: Rep. **35**, 1 (2001).
[46] G. Das, P. Blöchl, O. Andersen, N. Christensen, and O. Gunnarsson, Electronic Structure and Schottky-Barrier Heights of (111) $NiSi_2$/Si A- and B-type Interfaces, Phys. Rev. Lett. **63**, 1168 (1989).
[47] H. Fujitani and S. Asano, Schottky barriers at $NiSi_2$/Si (111) interfaces, Phys. Rev. B **42**, 1696 (1990).
[48] M. Lazzarino, G. Scarel, S. Rubini, G. Bratina, L. Sorba, A. Franciosi, C. Berthod, N. Binggeli, and A. Baldereschi, Al/ZnSe (100) Schottky-barrier height versus initial ZnSe surface reconstruction, Phys. Rev. B **57**, R9431 (1998).
[49] C. Berthod, N. Binggeli, and A. Baldereschi, Schottky barrier heights at polar metal/semiconductor interfaces, Phys. Rev. B **68**, 085323 (2003).
[50] W. Mönch, in *Electronic Properties of Semiconductor Interfaces* (Springer, 2004), p. 181.
[51] See the Supplemental Material at http://link.aps.org/supplemental/10.1103/PhysRevApplied.16.064064 for a complete discussion on band gaps and finite-size effects, including Refs [73–75], and for the LDOS and crystal structures for the following interfaces: β-Ga_2O_3(100)/H.OH/Pt(111), β-Ga_2O_3 ($\bar{2}$01) /Pt(111) with reduced strain, β-Ga_2O_3 ($\bar{2}$01) /Pt(221), and β-Ga_2O_3 ($\bar{2}$01) /Pt(321). We also include all the structure files (POSCAR) used to calculate the LDOS values presented in this paper.
[52] T. Oishi, Y. Koga, K. Harada, and M. Kasu, High-mobility β-Ga_2O_3 ($\bar{2}$01) single crystals grown by edge-defined film-fed growth method and their Schottky barrier diodes with Ni contact, Appl. Phys. Express **8**, 031101 (2015).
[53] S. Sze, C. Crowell, and D. Kahng, Photoelectric determination of the image force dielectric constant for hot electrons in Schottky barriers, J. Appl. Phys. **35**, 2534 (1964).
[54] Y. Yao, R. Gangireddy, J. Kim, K. K. Das, R. F. Davis, and L. M. Porter, Electrical behavior of β-Ga_2O_3 Schottky diodes with different Schottky metals, J. Vac. Sci. Technol. B, Nanotechnol. Microelectron.: Mater. Proc. Meas. Phenom. 35, 03D113 (2017).
[55] H. Fu, H. Chen, X. Huang, I. Baranowski, J. Montes, T.-H. Yang, and Y. Zhao, A comparative study on the electrical properties of vertical ($\bar{2}$01) and (010) β-Ga_2O_3 Schottky barrier diodes on EFG single-crystal substrates, IEEE Trans. Electron. Devices **65**, 3507 (2018).
[56] Q. He, W. Mu, H. Dong, S. Long, Z. Jia, H. Lv, Q. Liu, M. Tang, X. Tao, and M. Liu, Schottky barrier diode based on β-Ga_2O_3 (100) single crystal substrate and its temperature-dependent electrical characteristics, Appl. Phys. Lett. **110**, 093503 (2017).
[57] R. M. Gazoni, L. Carroll, J. I. Scott, S. Astley, D. Evans, A. J. Downard, R. J. Reeves, and M. W. Allen, Relationship between the hydroxyl termination and band bending at ($\bar{2}$01) β-Ga_2O_3 surfaces, Phys. Rev. B **102**, 035304 (2020).
[58] R. Anvari, D. Spagnoli, G. Parish, and B. Nener, Density functional theory simulations of water adsorption and activation on the (- 201) β-Ga_2O_3 surface, Chem. A Eur. J. **24**, 7445 (2018).
[59] Y. Ma, X. Zhao, M. Niu, W. Li, X. Wang, C. Zhai, T. Wang, Y. Tang, and X. Dai, Monoclinic Ga_2O_3 (100) surface as a robust photocatalyst for water-splitting, RSC Adv. **7**, 4124 (2017).
[60] J. H. Werner and H. H. Güttler, Barrier inhomogeneities at Schottky contacts, J. Appl. Phys. **69**, 1522 (1991).
[61] R. Tung, Electron transport at metal-semiconductor interfaces: General theory, Phys. Rev. B **45**, 13509 (1992).
[62] R. Tung, Electron transport of inhomogeneous Schottky barriers, Appl. Phys. Lett. **58**, 2821 (1991).

[63] P. Mazzolini, A. Falkenstein, C. Wouters, R. Schewski, T. Markurt, Z. Galazka, M. Martin, M. Albrecht, and O. Bierwagen, Substrate-orientation dependence of β-Ga_2O_3 (100), (010), (001), and $(2\bar{0}1)$ homoepitaxy by indium-mediated metal-exchange catalyzed molecular beam epitaxy (mexcat-mbe), Apl Mater. **8**, 011107 (2020).

[64] X. Zhou, H. Dong, and A.-M. Ren, Exploring the mechanism of water-splitting reaction in NiO_x/β-Ga_2O_3 photocatalysts by first-principles calculations, Phys. Chem. Chem. Phys. **18**, 11111 (2016).

[65] H. Mosbacker, Y. Strzhemechny, B. White, P. Smith, D. C. Look, D. Reynolds, C. Litton, and L. Brillson, Role of near-surface states in Ohmic-Schottky conversion of Au contacts to ZnO, Appl. Phys. Lett. **87**, 012102 (2005).

[66] M. Allen and S. Durbin, Influence of oxygen vacancies on Schottky contacts to ZnO, Appl. Phys. Lett. **92**, 122110 (2008).

[67] R. Schafranek, S. Payan, M. Maglione, and A. Klein, Barrier height at (Ba,Sr)TiO_3/Pt interfaces studied by photoemission, Phys. Rev. B **77**, 195310 (2008).

[68] T. Schultz, S. Vogt, P. Schlupp, H. von Wenckstern, N. Koch, and M. Grundmann, Influence of Oxygen Deficiency on the Rectifying Behavior of Transparent-Semiconducting-Oxide–Metal Interfaces, Phys. Rev. Appl. **9**, 064001 (2018).

[69] D. Guo, Z. Wu, Y. An, X. Guo, X. Chu, C. Sun, L. Li, P. Li, and W. Tang, Oxygen vacancy tuned Ohmic-Schottky conversion for enhanced performance in β-Ga_2O_3 solar-blind ultraviolet photodetectors, Appl. Phys. Lett. **105**, 023507 (2014).

[70] R. Lingaparthi, K. Sasaki, Q. T. Thieu, A. Takatsuka, F. Otsuka, S. Yamakoshi, and A. Kuramata, Surface related tunneling leakage in β-Ga_2O_3 (001) vertical Schottky barrier diodes, Appl. Phys. Express **12**, 074008 (2019).

[71] R. Lingaparthi, Q. Thieu, K. Sasaki, A. Takatsuka, F. Otsuka, S. Yamakoshi, and A. Kuramata, Effects of oxygen annealing of β-Ga_2O_3 epilayers on the properties of vertical Schottky barrier diodes, ECS J. Solid State Sci. Technol. **9**, 024004 (2020).

[72] J. Swallow, J. Varley, L. Jones, J. Gibbon, L. Piper, V. Dhanak, and T. Veal, Transition from electron accumulation to depletion at β-Ga_2O_3 surfaces: The role of hydrogen and the charge neutrality level, APL Mater. **7**, 022528 (2019).

[73] L. A. Cipriano, G. Di Liberto, S. Tosoni, and G. Pacchioni, Quantum confinement in group III–V semiconductor 2D nanostructures, Nanoscale **12**, 17494 (2020).

[74] A. D. Yoffe, Low-dimensional systems: Quantum size effects and electronic properties of semiconductor microcrystallites (zero-dimensional systems) and some quasi-two-dimensional systems, Adv. Phys. **42**, 173 (1993).

[75] Y. Kayanuma, Quantum-size effects of interacting electrons and holes in semiconductor microcrystals with spherical shape, Phys. Rev. B **38**, 9797 (1988).